

Performance results of laser-produced plasma test and prototype light sources for EUV lithography

Norbert R. Böwering
Igor V. Fomenkov
David C. Brandt
Alexander N. Bykanov
Alex I. Ershov
William N. Partlo
David W. Myers
Nigel R. Farrar
Georgiy O. Vaschenko
Oleh V. Khodykin
Jerzy R. Hoffman
Christopher P. Chrobak
Shailendra N. Srivastava
Imtiaz Ahmad
Chirag Rajyaguru
Daniel Golich
David A. Vidusek
Silvia De Dea
Richard R. Hou
Cymer, Inc.
17075 Thornmint Court
San Diego, California 92127

Abstract. Improved performance and specific results are reported for several test and prototype extreme ultraviolet (EUV) light sources developed for next-generation lithography. High repetition rate and high-power CO₂ laser-produced plasma sources operating on tin droplet targets are described. Details of laser architecture, source chambers and system operation are given. Stable output power, efficient light collection, and clean EUV transmission could be achieved for hours of operation. We review progress during integration of light sources with collector mirrors reaching EUV power levels at intermediate focus of 60 W and 45 W, respectively, with duty cycles of 25% and 40%. Far-field EUV images of the collected light were recorded to monitor the source output performance during extended tests of collector longevity and debris protection with system operation time exceeding 50 h. Development results on EUV spectra, out-of-band (OOB) radiation, and ion debris obtained with dedicated metrology setups are also described. Angle-resolved measurements with ion energy analyzer and Faraday cups reveal the contributions of individual ion charge states in related spectra. Our laser-produced EUV light source technology has now reached a level of maturity in full integration where prototype sources can be delivered and pilot line introduction can be prepared. © 2009 Society of Photo-Optical Instrumentation Engineers. [DOI: 10.1117/1.3224942]

Subject terms: EUV source; EUV lithography; laser-produced plasma (LPP); collector; plasma.

Paper 09044SSPRR received Mar. 9, 2009; revised manuscript received May 29, 2009; accepted for publication Jun. 2, 2009; published online Oct. 5, 2009. This paper is a revision of a paper presented at the SPIE Conference on Alternative Lithographic Technologies, February 2009, San Jose, California. The paper presented there appears (unrefereed) in SPIE Proceedings Vol. 7271.

1 Introduction

EUV lithography is the front-runner for next-generation critical dimension imaging, following after 193-nm immersion lithography for layer patterning below the 32-nm node. According to the International Technology Roadmap for Semiconductors (ITRS), high-volume manufacturing (HVM) could begin in 2013. Pilot line system introduction is then required as early as 2010. For EUV lithography, the availability of high-power 13.5-nm sources has been categorized as high risk and ranked as critical with other technologies requiring significant developments to enable the realization of EUV lithography. High-sensitivity photoresists with good line-edge-roughness (LER) and line-width-roughness (LWR) are needed to keep the required source power within reasonable limits. Photoresist sensitivity and other light absorbing elements are the basis to derive EUV source power requirements within the usable bandwidth (BW) of 2%. According to the joint requirements from scanner manufacturers,¹ an EUV power of >115 W with 2% BW at the intermediate focus (IF) is required for 5 mJ/cm² photoresist speed to enable >100 wph scanner throughput, and 180 W with 2% BW at IF is needed for

10 mJ/cm². Photoresist sensitivities above 20 mJ/cm² could drive power requirements well above the 200-W level, and the need for a spectral purity filter (SPF) could increase the requirements even higher. A scalable EUV source architecture is needed to enable the evolution of EUV lithography during the life cycle of the technology. A comprehensive review of EUV source developments for lithography is given in Ref. 2. Following the early development of discharge-produced plasma (DPP) sources, laser-produced plasma (LPP) sources have now taken the lead and are expected to deliver the necessary high power for critical-dimension HVM scanners for the production of integrated circuits in the post-193-nm immersion era.

LPP systems have many advantages over low-power DPP sources. The drive laser power is scalable through increase of repetition rate and pulse energy, making it easily extendable to even higher powers for future generations of EUV scanners and also allowing compensation of photoresist sensitivity limitations. The high conversion efficiency (CE) of CO₂ and Sn enables the required EUV power levels for HVM to be achieved at relatively low laser power so that reasonable laser costs can be realized. The isolated plasma in the central region of the source chamber provides large distances between the hot plasma and cham-

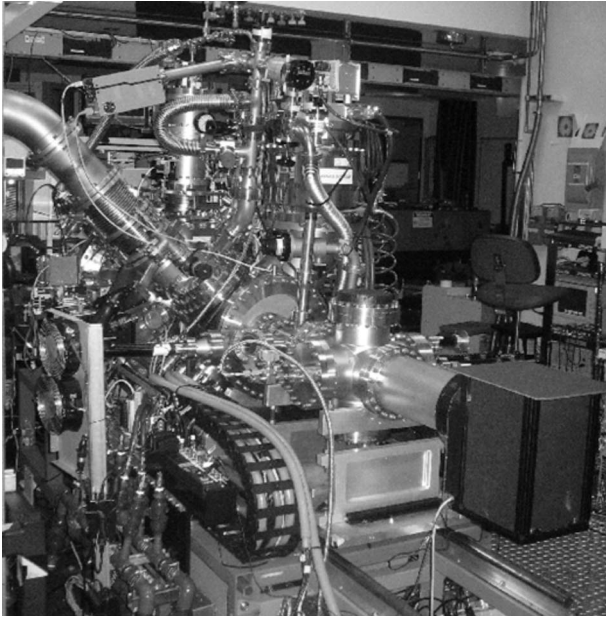


Fig. 1 Photograph of LT1 development system.

ber components. There are no electrodes; hence, there is no need for elaborate and expensive electrode cooling, nor is there any electrode debris as observed in DPP sources. The small etendue of an LPP source significantly reduces the complexity of optical system designs and supports illuminators with variable sigma and advanced illumination techniques such as annular, dipole, or quadrupole. Mass-limited usage of targets is made possible with droplet generator designs, creating very small droplet diameters leading to little debris generation. Normal incidence (NI) collector mirrors exhibit good thermal load capacity and greater image fidelity under high heat load. The multilayer mirror (MLM) coating provides substantial spectral filtering of out-of-band (OOB) EUV radiation. In addition, the MLM coating can be stacked, or the number of layer periods can be increased, providing sacrificial layers that extend the useful lifetime of the NI collector and enable a low-cost operation of the source in an HVM environment. The goal of our development efforts at Cymer is to provide a cost-effective, high-power LPP EUV light source that meets all requirements for EUV lithography in production for post-193-nm technology and that supports specific exposure tool designs of individual lithography customers.

2 LPP Development System Descriptions

Our research and development system, called the life-test 1 (LT1) system, was described in detail previously.^{3,4} Irradiation of tin droplet targets by tightly focused high-power CO₂ laser pulses leads to evaporation and high ionization of tin atoms that efficiently emit EUV photons that are collected and delivered to the source output region. A photograph of the source chamber is shown in Fig. 1. The LT1 serves as the primary tool to test the fundamental capability and longevity of production designs. The performance is monitored by metrology directed at both plasma and intermediate focus positions. A multilocation witness sample holder at the position of the collector is used to acquire life

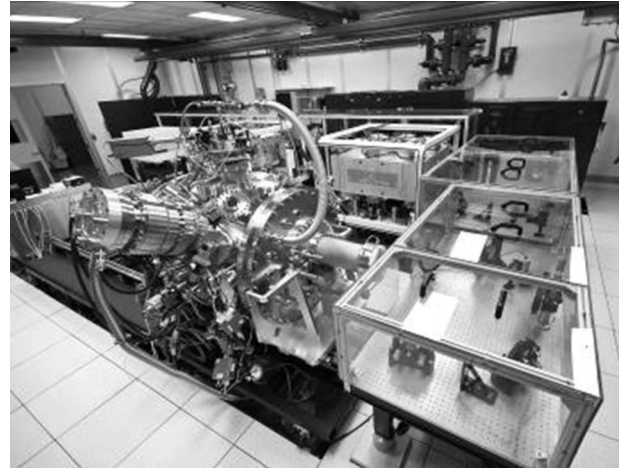


Fig. 2 View of prototype source system in manufacturing test bay.

test data on various MLM samples, allowing the effectiveness of the debris mitigation and reflectivity of the MLM coatings to be evaluated quantitatively. Alternatively, a sub-aperture collector mirror with 1.6 sr collection angle can be installed. Integrated controls permit semiautomatic operation of the system as well as monitoring and data collection from the various metrology instruments attached to the LPP chamber.

Several manufacturing bays for production of prototype and pilot LPP sources with class 10,000 clean-room space were also completed in recent months. Following installation and extensive testing of the drive laser system and other major system components, several source prototypes are now being assembled; the first production system for shipment to a customer is already fully integrated with its collector and debris mitigation subsystems. The water-cooled chamber of the production systems is larger in diameter compared to the development system in order to house a full-size 5-sr collector. The optical elements are water-cooled to enable high-power operation. Other system components like laser beam transport, support frame, vacuum pumping, droplet generation, controls, and monitoring were also significantly expanded and improved to meet production requirements. A photograph of a prototype source system in its manufacturing bay is shown in Fig. 2. The full-size high-duty cycle source system described here is called Proto1.

The source systems are accompanied by a pulsed high-power RF pumped CO₂ laser system (~11-kW power) operating at a wavelength of 10.6 microns and repetition rates of typically 50 kHz. (Ref. 5) Figure 3 gives an overview of the subsystem components on the LT1 source chamber. The laser beam enters the vacuum chamber through an entrance window and is focused onto the target through a central hole in the collector mirror. The focusing system is highly accurate with active beam steering, producing a beam waist at the target site of approximately 150 microns in diameter. The target site is located at the primary focus of an elliptical collector optic with the other focus, called intermediate focus (IF), located at the output region of the interface with the scanner.

A liquid tin (Sn) droplet generator is positioned at the

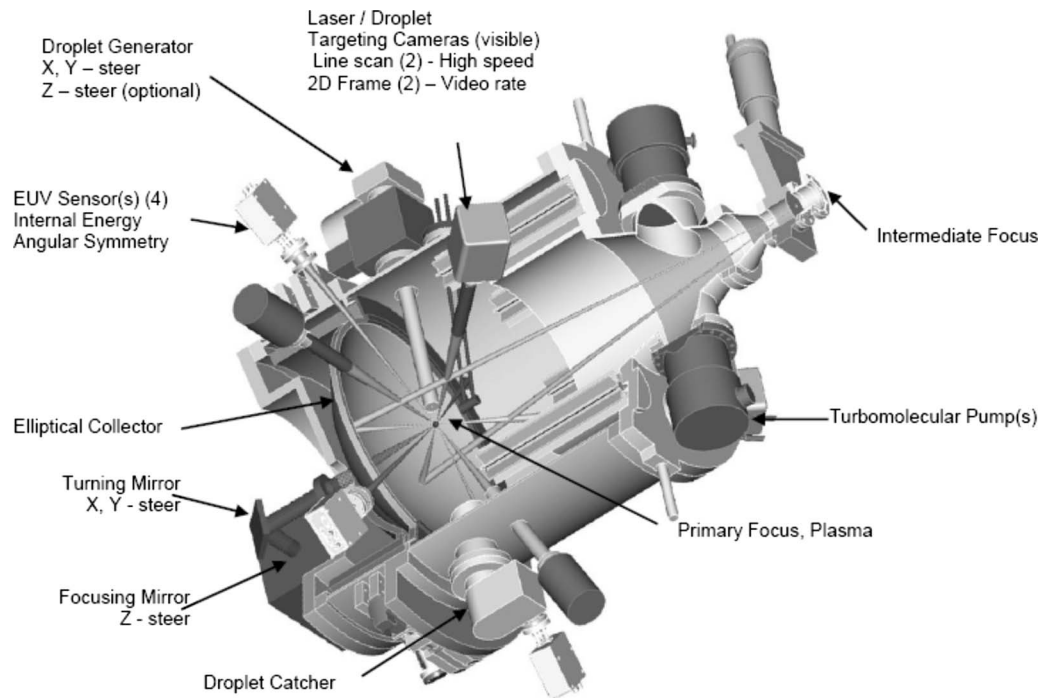


Fig. 3 Drawing of EUV LT1 source chamber with subsystems.

chamber. It produces droplet sizes from 50 to 30 microns in diameter at repetition rates of about 50 kHz. Droplet speed capability is in excess of 30 meters per second, with interdroplet timing stability better than 0.2% of the period. Unexposed droplets are caught and disposed of in a droplet catcher system. Droplet position in X and Z (Z is the CO_2 beam direction, and X is the horizontal axis perpendicular to the laser beam) is controlled with a closed-loop steering system using a feedback signal from targeting charge-coupled device (CCD) cameras. Calibrated EUV sensors positioned at several angles with respect to the X - Z plane and laser beam direction measure the 2% bandwidth EUV energy produced by each pulse. Turbomolecular pumps are employed for evacuation of the chamber; system base pressures in the range of 10^{-6} Torr or less can be achieved.

When irradiated by the laser, each tin droplet is evaporated, ionized, and heated to the optimal temperature where the plasma produces EUV photons most efficiently. The EUV photons emitted in the direction of the CO_2 laser are reflected off a multilayer coated ellipsoidal mirror covering about 1.6-sr (>5 sr on production systems) solid angle, focusing the energy to the IF, where an aperture and metrology devices are placed to measure the quality of light in the far field. Debris mitigation is incorporated to protect the multilayer coating on the collector from high-energy ions and other particles emitted from the plasma. Faraday cup (FC) sensors and MLM witness samples can be used together when mounted on a holder, replacing the collector to measure ion energies and ion damage to the coating. In addition to visible CCD cameras for controls, pinhole camera devices with EUV-sensitive detection are also incorporated to view the plasma emission region and measure the size and stability of the EUV emitting region. Throughout this paper, we report powers measured with EUV detectors

at plasma, transformed to IF-equivalent EUV powers using standard assumptions of 50% reflectivity for a 5-sr collector and 90% optical transmission from plasma to IF.

3 High-Power CO_2 Laser

The overall system architecture is shown in Fig. 4. The high-power CO_2 drive laser has been under development during the last years and has undergone a series of design revisions with several architecture modifications in order to optimize its performance. A brief description of our pulsed CO_2 laser developments has been given previously.⁵ A three-stage system comprised of three laser amplifier cubes separated by optical isolation devices is used. The infrared (IR) laser pulse is propagated through nearly 50 m of optical path with many (>200) optical elements used to condition and guide the beam before it enters the vacuum vessel to interact with the Sn droplet to produce EUV radiation. A beam transport and focusing system achieves the final tight focusing to within $150\ \mu\text{m}$ diameter. An image of the beam focusing is shown in Fig. 5. Due to the high number of optics, the beam does not have a fully Gaussian profile. The measured M^2 of the optimized beam is approximately 2. Improvements to the beam quality are made by incorporating spatial filters into the beam path and by using optics with higher surface quality compared to standard CO_2 laser optics. Furthermore, for the production-type CO_2 drive laser, all optics are water-cooled and solidly mounted.

4 LPP EUV Development Results

Using the LT1 development system described earlier, the output performance of the LPP light source was successively improved in terms of average power level by in-

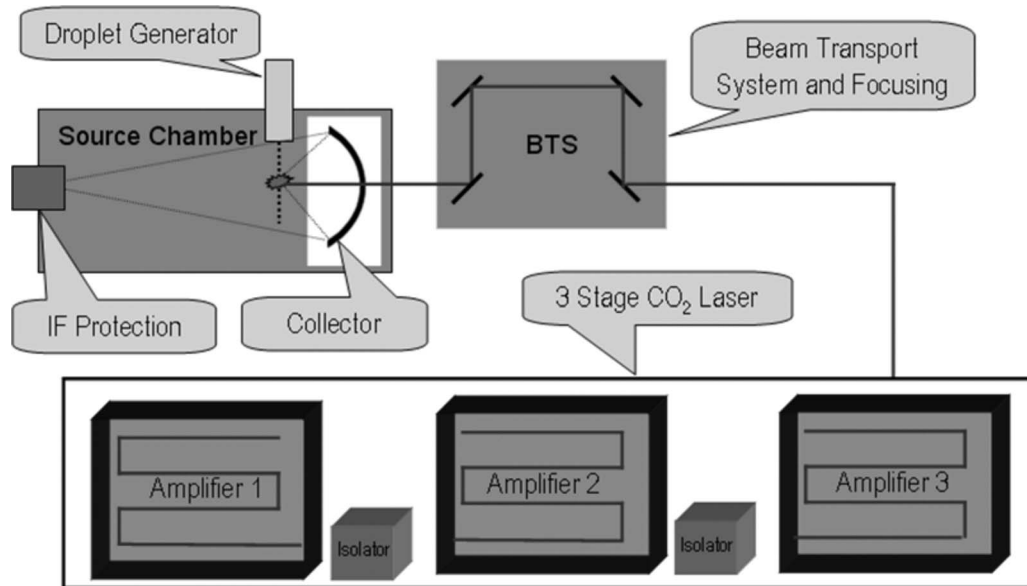
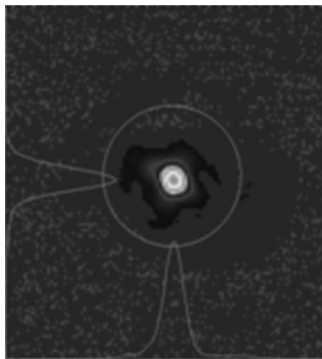


Fig. 4 Laser-produced plasma system architecture.

crease of duty cycle and duration of operation through incremental improvements of stability and thermal control. Initial testing was carried out using bursts of 1-ms duration, up to ~30% duty cycle and 50-kHz pulse repetition rate. IF equivalent power levels could be increased up to about 40 W, with measurements carried out at plasma using standard assumptions of 50% reflectivity for a collector with 5-sr collection angle and 90% optical transmission through the source.³ Initially, there were limitations for extended operation at high duty cycles due to the occurrence of thermal lensing phenomena in the optics used. These thermal restrictions were overcome by means of water-cooled optic mounts, and the system was ramped up with successively longer operation to hours of continuous runtime. A further improvement was achieved by changing the burst pattern to a mode that is more characteristic for the intended use in the exposure tool. The burst length was increased from milliseconds to bursts of seconds in duration. Figure 6 gives a comparison of CO₂ laser power and corresponding in-band EUV output power versus time for operation of the LT1 source in a 400-ms burst at 40-kHz repetition rates. Typi-

cally, IF-equivalent EUV powers in the range of 60 W are obtained in open-loop operation without energy control and at low duty cycles (~1%). A strong correlation between incident CO₂ laser power and EUV output power is observed.

Using such burst lengths of 400-ms duration, the prototype system was operated at 80% duty cycle. Long-term high-power operation is required to support high wafer throughput at the exposure tool. Extended operation of the Proto1 source for 18 h at IF-equivalent power levels of above 20 W was demonstrated successfully. The total accumulated EUV dose at IF determined from the measured EUV power at plasma using standard assumptions corresponds to about 1 MJ. Such dose levels should be sufficient for the exposure of a batch of approximately 250 wafers of



Beam quality: ($M^2 \sim 2$)

Fig. 5 Image of CO₂ laser focal spot.

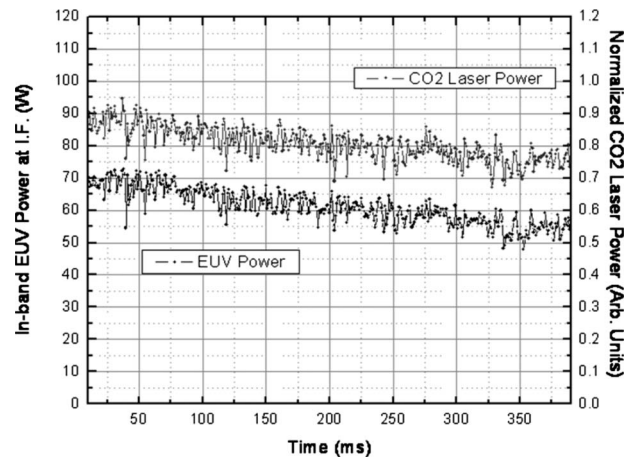


Fig. 6 Normalized CO₂ laser power and in-band EUV power versus time for 400-ms burst duration at 40 kHz (LT1). Each data point represents the integral over 40 pulses.

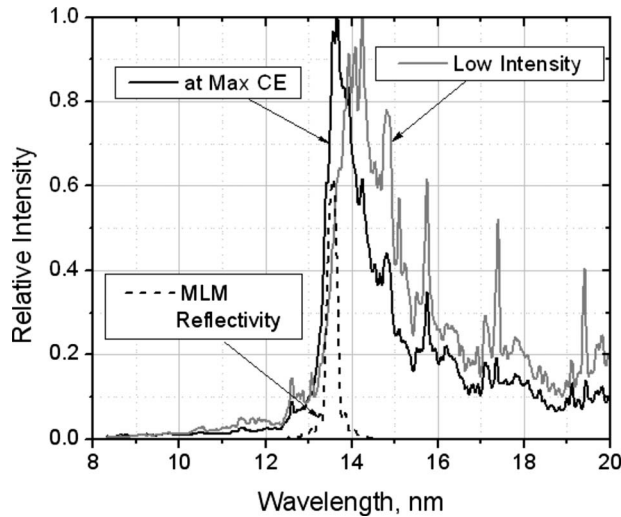


Fig. 7 EUV spectra measured at optimal laser intensity (maximum CE) and at lower intensity in comparison.

300-mm size. Further EUV power increase is planned to reach required dose delivery levels in excess of several MJ per day.

The measured spectra at various intensities of laser radiation confirm that the optimum plasma parameters are reached at maximum observed CE. Figure 7 shows EUV spectra at optimal intensity (black curve) and at intensities approximately four times less than optimal (gray curve) in direct comparison. The spectra were recorded using a low-repetition-rate CO₂ laser system and a flat-field EUV spectrometer described previously.⁶ The optimal spectrum matches the reflectivity curve of MLM coating of the collector (dashed line) very well, with very small OOB EUV radiation. When the laser intensity is less than optimal, the plasma temperature is also less than optimal, and the spectrum shifts to longer wavelengths. When the laser intensity exceeds the optimal value, the spectral emissions indicate an elevated plasma temperature above the optimal value, but this variation is less pronounced and therefore not shown in the figure.

5 Tests of the Far-Field Image

Behind the IF region, several important measurements of the EUV output characteristics from the source can be performed. At a distance of several 10 cm behind IF, the EUV intensity distribution can be intercepted in order to obtain information about source power, angular distribution, and its stability, as well as on collector reflectance and collector defects. This plane represents a far-field (FF) distribution of EUV radiation. The shape and intensity of the EUV distribution can be used for precise positioning of the source plasma in the focal point of the collector. We have developed some metrology concepts for characterization of the FF distribution. A schematic setup of our diagnostic is shown in Fig. 8.

A fluorescent converter screen is placed at ~ 27 cm behind IF; the generated visible light is monitored with a CCD video camera behind a vacuum window. The fluorescent converter screen is composed of a Ce:YAG crystal coated with thin films of Zr (150 nm thick) and Si (25 nm thick). Future designs will employ multiple screens with the possibility to perform measurements in FF at distances significantly longer than 20 cm. The transmission of the coating together with the MLM coating of the collector provides a good spectral selection for EUV radiation. However, it has to be kept in mind that the radiation bandwidth after a single reflection from the collector ($\sim 4\%$) is wider than that obtained from multiple reflections of further EUV optics ($\sim 2\%$), which gives some uncertainty to the corresponding intensity distribution into 2% bandwidth.

The progress on the manufacturing of near-normal incidence collector mirrors with graded multilayer coating has been described in detail previously.^{7,8} Several subaperture collector mirrors with 1.6-sr collection angle (~ 300 mm diameter) are available for use with the LT1 source. In addition, the infrastructure is now in place for the production of large-size (>650 mm diameter) collector mirrors, and substrates have been coated with graded multilayer coatings with layer periods optimized for high EUV reflectance at the corresponding incidence angles. Typically, average EUV reflectivities above 40% for unpolarized light were reached.

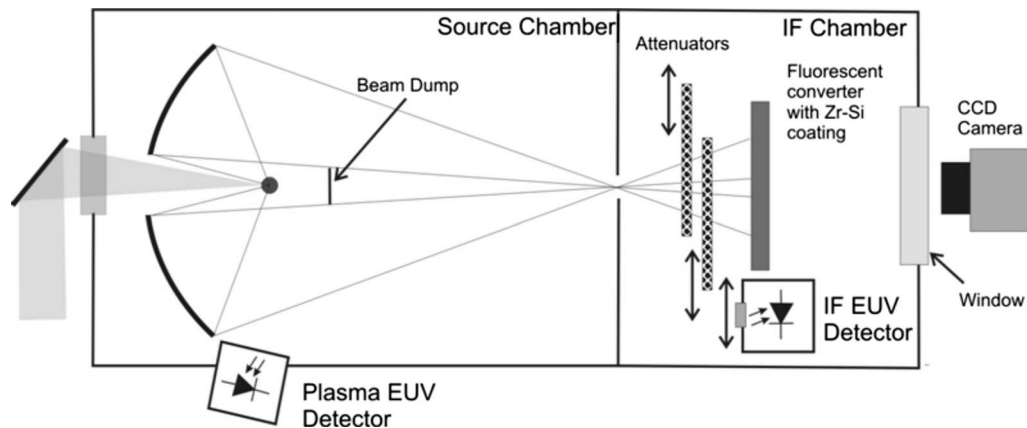


Fig. 8 Schematics of diagnostic setup for far-field measurements. A fluorescence converter and CCD camera are used for image recording behind IF; attenuators can be inserted for power reduction. Photodiode-based EUV detectors are employed to determine power at plasma and converter calibration.

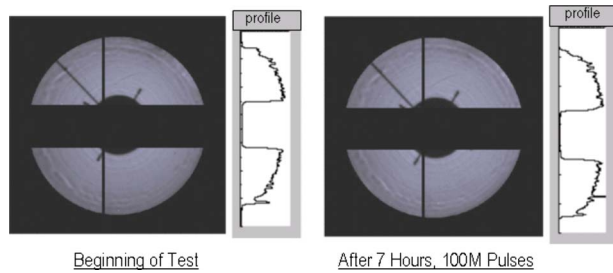


Fig. 9 Image of LT1 collector in the far field and corresponding scan of radial intensity profile. The left figure shows the result at the beginning of the test run; the right figure shows the respective data after 7 h of operation, corresponding to 100 million pulses.

Using subaperture collector mirrors and the IF imaging configuration on LT1, extended longevity runs are carried out to assess the behavior of imaging and reflectance properties of the collector and of the effectiveness of debris mitigation schemes. Figure 9 shows FF images recorded with the fluorescence converter detector behind IF at the beginning of a test run and after 7 h of continuous operation, corresponding to an accumulation of about 100 million pulses. Within the noise of the data, no significant change in the distribution pattern and radial intensity profile can be detected. The observed ring-shaped intensity variations of the FF intensity pattern are attributed to surface roughness deficiencies of the collector substrate.

The LT1 setup with mounted collector mirror was also used to test the effectiveness of debris mitigation schemes. One debris mitigation subsystem addresses multilayer erosion by significantly reducing the ion flux incident at the mirror surface by up to four orders of magnitude, and the ion energy by about an order of magnitude.⁵ Erosion can also be addressed by adding sacrificial multilayers during the coating step of collector fabrication. A second debris mitigation subsystem eliminates tin deposition, which is critical because a deposited tin layer with a thickness of only about 1 nm results already in unacceptable reflectivity reduction by absorption of the EUV radiation. The debris mitigation technology was initially developed and validated on the LT1 system using both witness samples and subaperture 1.6-sr collectors. Figure 10 shows a test example of debris mitigation technologies with collector mirror where ~40 W of EUV power was measured at plasma over 51 h

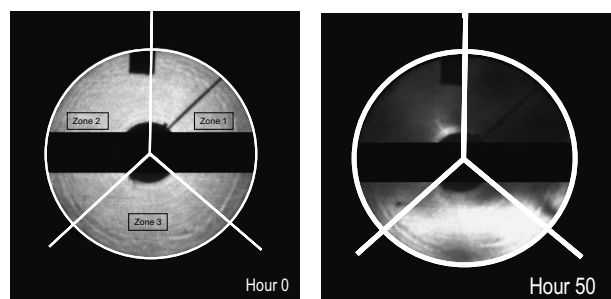


Fig. 10 Far-field EUV intensity distribution of subaperture collector during debris protection testing at the beginning of test and after 50 h (LT1). Zone 3 shows only very slight degradation, attributed mainly to infringement from neighboring zones.

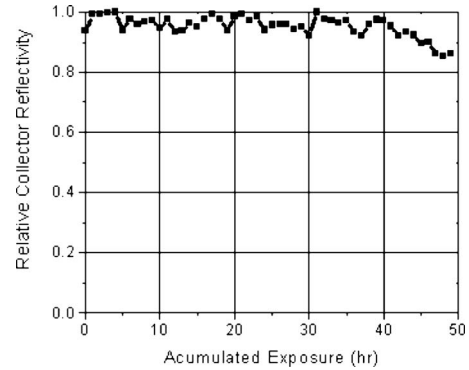


Fig. 11 Relative reflectivity of zone 3 determined from IF data in relation to the EUV power monitor data at plasma (LT1).

of operation at 25% duty cycle and 1-ms burst length. Three different collector protection geometries were employed for different sections of the surface area in order to accelerate the testing. Zones 1, 2, and 3 were each configured differently. Zones 1 and 2 showed some degradation relatively early in the test and continued to give reduced image intensity during the remaining hours. On the other hand, zone 3 did not show a significant reduction until almost 40 h into the testing. After 40 h of exposure, zone 3 also began to degrade, as is shown in the 50-h exposure image in Fig. 10. It is believed that this reduction was in part influenced by encroachment from zones 1 and 2. Figure 11 shows the relative reflectivity of a 3 cm × 3 cm area of zone 3 as viewed from IF with the fluorescence converter and compared to an EUV monitor measuring EUV power at plasma, as indicated schematically in Fig. 8. The relative reflectivity stays nearly constant for the first 40 h and then begins to decline. Zone 3 geometries were ultimately determined to be successful and were transferred to our production system design.

Further testing of the far-field EUV distributions behind IF have now started on the prototype source using the full-size (>650 mm diameter) collector mirrors with 5-sr collection angle. Figure 12 shows the first results for such a fully integrated production EUV source-collector system (Proto1). The far-field intensity distribution was recorded with a similar detection arrangement as shown in Fig. 8, but adapted to the changed geometry (compared to LT1) with larger EUV light cone. A slight misalignment of horizontal obscurations as well as a small residual tilt angle leading to some clipping of the image on one side can be discerned; however, these minor deficiencies will be easily correctable during future testing. More concerning is the observation of nonuniform ring-shaped intensity variations in the image that can most likely be attributed to surface imperfections of the particular collector substrate used in this test. The prototype system was operated with bursts of 400-ms duration at 40% duty cycle. Figure 13 shows the corresponding measured 45-W to 50-W average EUV power level obtained under these conditions for a sequence of consecutive bursts. These results represent a major milestone in our integration efforts and show that the EUV light source development is well under way to meet the demanding requirements for first prototype production and pilot EUV illumination systems.

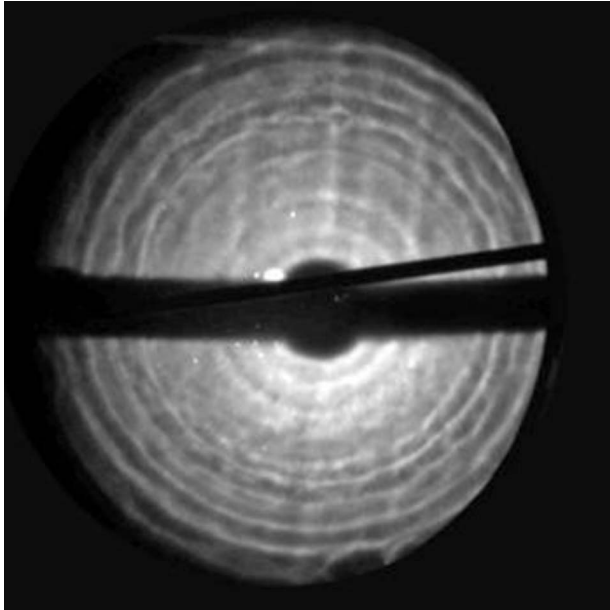


Fig. 12 Far-field EUV intensity distribution of 5-sr collector (Proto1).

6 Out-of-Band (OOB) Contributions

OOB radiation in bands with high MLM reflectivity [deep ultraviolet (DUV) from 300 to 400 nm and far IR beyond 1.5 μm] may cause either undesirable exposure of photoresist (for the UV–DUV range) or additional heating of the wafer and mask (in the case of the IR band). For OOB measurements, several different tools were used. Currently, spectrometers for measurements of spectra for most regions from 6-nm to 1000-nm wavelength are available. For the range from 6 nm to 22 nm, we use a grazing-incidence spectrometer.⁶ The sensitivity of the spectrometer is calibrated at 13.5 nm with an absolute EUV in-band detector. The EUV in-band energy measured with the spectrometer correlates with the EUV energy detector to a high degree of accuracy.

For the UV, visible, and near-infrared (NIR) regions, three miniature spectrometers (Ocean Optics) equipped with individual fiber optics were used. The absolute sensitivity of the spectrometers was initially calibrated with a standard solar spectrum and later recalibrated with a cali-

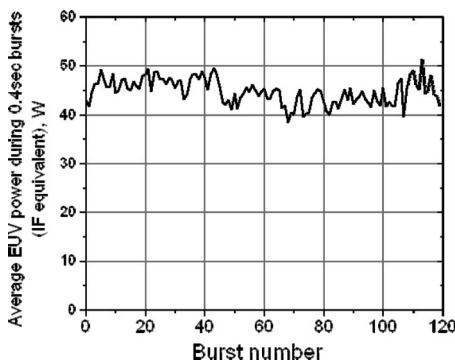


Fig. 13 EUV power measured during 120 bursts of 400-ms duration (Proto1).

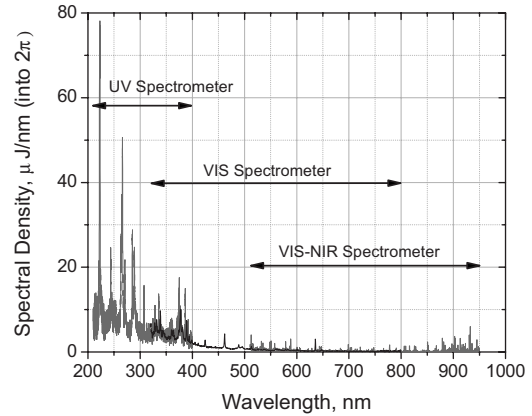


Fig. 14 OOB radiation measurements extended from 950 nm down to 220 nm.

bration tool (DH-2000-CAL). The shortest wavelength in the solar spectrum that may be used for absolute sensitivity calibration is at a wavelength of 320 nm. Employment of this calibration tool enabled us to extend our calibrated measurements down to 220 nm. A calibrated PEM-L detector was employed for measurement of reflected radiation at 10.6 μm.

UV, visible, and near-infrared spectra have been measured at optimal laser intensity in a setup with low-repetition-rate CO₂ laser on flat targets with the three spectrometers. After calibration of the spectrometers with the solar spectrum and the calibration tool, the spectral intensity was obtained in absolute units (μJ/nm into 2π solid angle) assuming a uniform angular distribution of the radiation. The resulting spectra are presented in Fig. 14. The overlapping bands of the spectra measured with different spectrometers coincide with a high degree of accuracy.

Figure 15 shows measured spectral density versus wavelength on a semilogarithmic plot. The open and solid squares show measurements obtained by using the DH-2000 and the solar spectrum for calibration. The measured values fit well to an exponential line. Extrapolation of the line to the region from 100 to 220 nm enables an estimation of the OOB radiation for this region. This shows that in

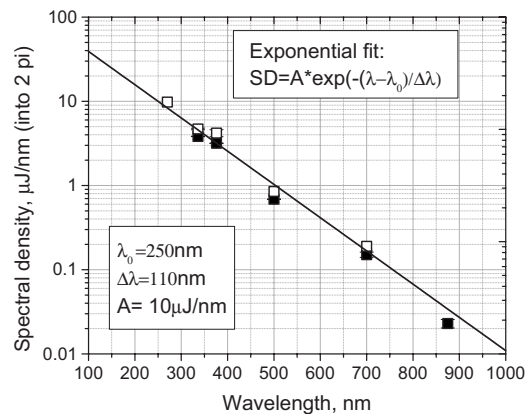


Fig. 15 Extrapolation of OOB radiation into the DUV region. It is estimated that the DUV contribution is about 40 to 70% of the in-band EUV contribution.

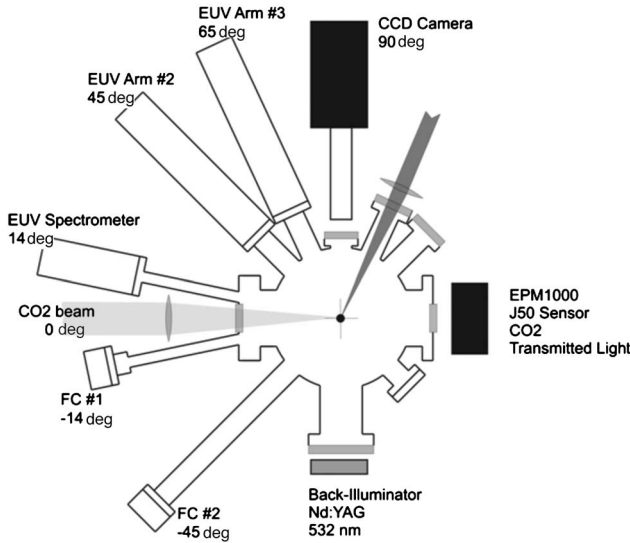


Fig. 16 Low repetition rate setup with diagnostic tools for CE optimization and ion energy distribution measurements.

the 130 to 400 nm band, the OOB contribution from plasma is 40 to 70 % of the EUV in-band radiation intensity. This may imply that a spectral purity filter is required for an LPP EUV source.

7 Ion Debris Measurements

The main process responsible for collector reflectivity degradation is sputtering of the collector by the high-energy ions generated from the plasma. Previously, we presented the characterization results for the protection technique developed for attenuation of flux and energy of the ions before they reach the collector.⁵ These experiments were performed with a Faraday cup (FC) installed at 45 deg to the laser beam direction. The polar angles of EUV radiation and ion flux for the HVM tool collector range from 16 to 80 deg (angle measured with respect to the laser beam). For confident design of the HVM tool and optimization of the protection technique, we also conducted ion characterization at small (14 deg) and medium (45 deg) angles. The goal of the characterization was to check whether the ion energy distribution at small angles differs significantly from the one at medium angles. We do not expect the ion energy and flux to increase for angles larger than 45 deg.

For the ion energy distribution, we used the low-repetition-rate experimental setup. The measurements were conducted on droplets at the conditions corresponding to high CE (above 3% in-band into 2π). This setup is shown schematically in Fig. 16.

The apparatus is equipped with all required subsystems (including droplet generator, back-illumination, etc.) and diagnostic tools. The diagnostics include two EUV energy measurement detectors (mounted at 45 deg and 65 deg with respect to the incident laser beam), an EUV spectrometer, and two Faraday cups (Kimball Physics, FC-73A) for ion energy distribution measurements at the angles of 14 deg and 45 deg at a distance of 43 to 46 cm from plasma. The energy of the CO₂ laser beam was measured time-resolved with the PEM-L IR detector that was calibrated with a J-50

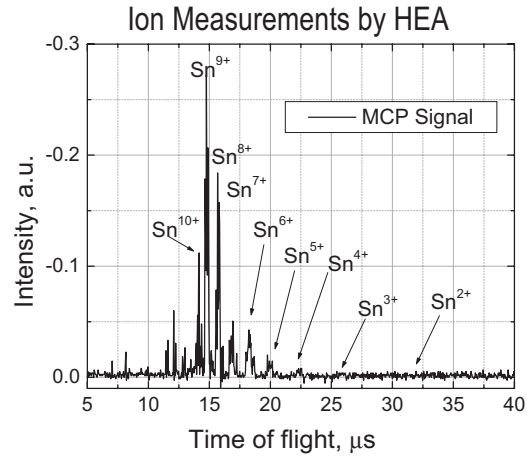


Fig. 17 Sn ion time-of-flight distributions confirming that the conditions are optimized for high EUV CE.

pyroelectric detector. A ZnSe window was used as a chamber output window to measure the transmitted laser light in the case of droplet targets. A hemispherical energy analyzer (HEA) was sometimes also connected to the setup (not shown in Fig. 16). For given voltage applied to the HEA electrodes, only ions with a given E/Z ratio are transmitted. The wave form signal from the multi-channel plate (MCP) detector enables to separate ions with different energy by time-of-flight measurement. Thus, the HEA provides information about ion energy and charge. For absolute measurements of the ion flux intensities, a calibration of the MCP sensitivity for the various ion energies is required. Ions emitted from the plasma at optimal laser intensity were characterized with both HEA and FC detection. The ion time-of-flight measurement results are presented in Fig. 17.

The HEA measurements showed that a significant number of ions originating from the plasma have a charge Z in the range from 8 to 10. These ion states of Sn radiate photons with wavelengths close to 13.5 nm. Thus, the ion composition characterization confirms that the plasma conditions are near optimum for high EUV in-band radiation.

The FC detectors were configured for ion detection by applying a negative voltage of 30 to 50 V to the suppression grid in order to reduce the influence of secondary electrons emitted from the collector (see Fig. 18). The collector was loaded with a resistor of 1 kOhm. For simple measure-

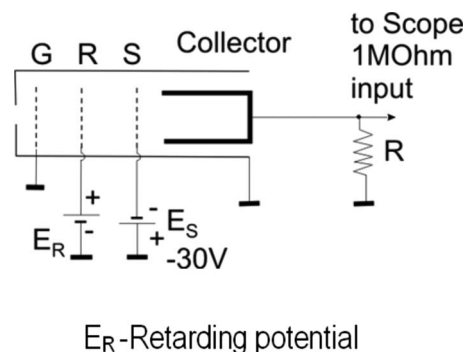


Fig. 18 Schematics of the Faraday cup measurement tool.

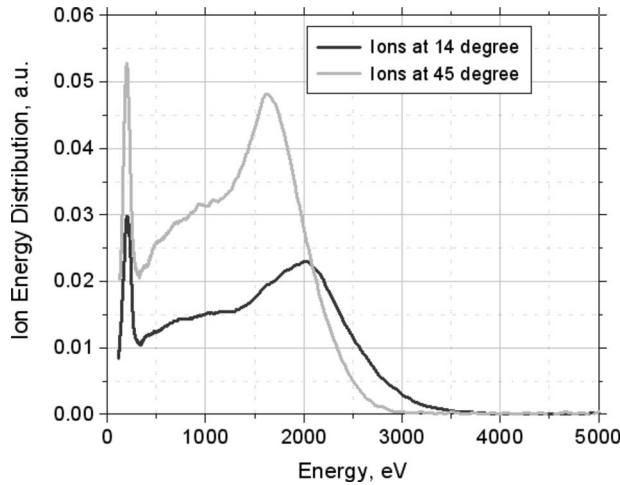


Fig. 19 Measurements of ion energy distributions at 14 and 45 deg with respect to the laser beam.

ments, the retarding grid of the FC was grounded. For ions of the same charge state Z , the FC waveform signal $U_i(t_i)$ is proportional to the absolute velocity distribution of ions $\varphi(v)$, where the velocity is defined by the time of flight t_i , and distance from plasma to the FC collector L . In our case, we have ions with various Z ; thus, the signal should be normalized to the charge state (or average Z), because the ions carry a charge proportional to Z . For conversion of the FC signal into the energy distribution function $f(\varepsilon)$, we converted velocity to kinetic energy, assuming that all ions have a mass of $M=118.7$ a.u. The FC voltage signal U_i is proportional to the absolute velocity distribution function and should be multiplied by the derivative of velocity by energy for proper conversion to the energy distribution function. After simple transformations, we obtain that the conversion is given by the multiplication of the voltage by the time of flight:

$$f(\varepsilon) = \varphi[v(\varepsilon)] \cdot \frac{dv}{d\varepsilon} = \varphi[v(\varepsilon)] \frac{1}{\sqrt{2M\varepsilon}},$$

where

$$v(\varepsilon) = \sqrt{\frac{2\varepsilon}{M}}, \quad v_i = \frac{L}{t_i}, \quad \varphi(v_i) \propto U_i(t_i),$$

$$f(\varepsilon_i) \propto U t_i, \quad \varepsilon_i = \frac{M v_i^2}{2}.$$

The typical ion energy distribution functions obtained with droplet targets from processed FC waveforms are shown in Fig. 19 for two angles (14 deg and 45 deg). The maximum energy observed at small angle ($E_{max}=3.5$ keV) is slightly higher than the one observed at 45 deg angle ($E_{max}=3.0$ keV). The peak of the energy distribution is at $E_{peak}=2.0$ keV for small angles and $E_{peak}=1.6$ keV for 45 deg. The ion flux at small angle is approximately two times less compared to the one at 45 deg, although the diagnostic tools were identical (same apertures, distances, and electronics).

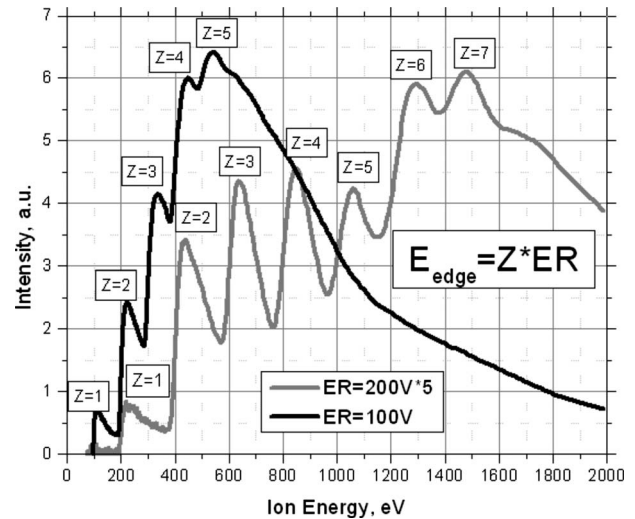


Fig. 20 Ion charge state measurements. Wave form converted to the energy scale shows cutoff edges of ions with different Z . Ions with $Z=7$ and below are well distinguished.

Faraday cup measurements show the ion intensity as a function of energy. The peak of the distribution is at approximately at 1.5 to 2 keV; the highest observed energies in the spectrum were 3.0 to 3.2 keV. The high-energy threshold was limited by the short distance from plasma to Faraday cup (16.5 cm). Transient relaxation processes from initial photons/electrons generate a negative spike on the wave form. Previously, the ion characterization was made at a four times larger distance to the detector such that the positive pulse of ions was distinctly separated from the initial negative spike. However, most of the ions had energies less than 3 keV for CO_2 laser intensities close to optimum for high EUV generation.

As was discussed in more detail previously,⁵ when debris mitigation was applied for ion flux attenuation, the flux was reduced by four orders of magnitude and the maximum observed energy in the spectrum was less than 300 eV, with a peak value at approximately 200 eV. These results demonstrate the extremely high efficiency of the developed technique. This will mitigate the action of ions on the MLM collector significantly and achieve an economically attractive lifetime of the collector mirror coating. The transmission of the debris mitigation for EUV light was also measured and found to be more than 80%.

Further measurements on the characterization of the ion state with the FC were carried out on flat targets. A retarding potential E_R was applied to the retarding grid of the FC (see Fig. 18), and the recorded wave forms were processed according to the algorithm described earlier. The original wave forms had a saw tooth shape at high times-of-flight corresponding to low ion velocities. When the wave forms were converted to the ion energy distributions, the saw tooth structure revealed well-distinguished low-energy cut-off edges corresponding to ions with various Z states. The edge position is equal to the retarding potential multiplied by the Z number ($Z=1, 2$, etc.). The ion energy distributions are shown in Fig. 20. Ions with Z up to 7 can be

distinctly observed. In order to obtain the number of ions for given Z , the presented distribution should be divided by Z . This type of processing is somewhat complicated by influences of neighboring ion states. Information about the charge states of the ions coming from the plasma is an important aspect for the optimization of debris protection techniques.

8 Conclusions

The laser-produced plasma EUV source has been shown to be the most viable source technology with high scalability to meet requirements from leading scanner manufacturers and to provide a path toward higher power as the lithography tools evolve over their life cycle. Progress achieved on the development of subsystems described in this paper enabled us to demonstrate high stability of EUV energy at high average powers and increased duty cycles. The collector longevity was tested with a 1.6-sr mirror that revealed no erosion of the MLM layers during 7 h of continuous operation. Stable transmission of EUV power to IF and good far-field EUV intensity distribution was obtained. Debris protection geometries were tested during more than 50 h of collector exposure at 25% duty cycle. As a major milestone, a fully integrated source module with large-size collector was operated at 45 W of EUV power. Measurements of EUV spectra and out-of-band spectra were carried out. Characterization of ions generated by the plasma was performed at small angles. Separation of ions with different charge state was demonstrated with Faraday cup diagnostics. These investigations were aimed at the optimization of the balance between debris mitigation techniques and cleaning techniques for the collector.

Cymer is committed to commercializing an HVM EUV light source for the sub-32-nm node and continues to meet its source development schedule. The LPP source technology has reached a state of considerable maturity, with full system integration to enable the IF power levels required for production-type light sources and for the preparation of pilot line systems. With future continued progress of EUV average output power, the LPP technology can provide the much needed margin in balancing photoresist sensitivity, optics degradation, process latitude, and overall equipment throughput. The laser-produced plasma technology is our chosen technology path for HVM EUV lithography applications.

Acknowledgments

The authors gratefully acknowledge the valuable contributions from Martin J. Neumann and David N. Ruzic of the University of Illinois, Urbana-Champaign; Marco Perske, Hagen Pauer, Mark Schürmann, Sergiy Yulin, Torsten Feigl, and Norbert Kaiser of Fraunhofer Institut f. Angewandte Optik und Feinmechanik; Eric Gullikson and Farhad Salmassi of Lawrence Berkeley National Laboratory; Frank Scholze, Christian Laubis, Christian Buchholz, and coworkers at PTB; Steven Grantham and Charles Tarrío of the National Institute of Standards and Technology; and Mark Tillack and Yezheng Tao of the University of California at San Diego. We are also very thankful for the

invaluable support and contributions, past and present, of many scientists, engineers, and technicians involved in the EUV technology program at Cymer.

References

1. K. Ota, Y. Watanabe, V. Banine, and H. Franken, "EUV source requirements for EUV lithography," in *EUV Sources for Lithography*, V. Bakshi, Ed., pp. 27–43, SPIE Press, Bellingham, WA (2005).
2. V. Bakshi, Ed., *EUV Sources for Lithography*, SPIE Press, Bellingham, WA (2005).
3. D. C. Brandt, I. V. Fomenkov, A. I. Ershov, W. N. Partlo, D. W. Myers, N. R. Böwering, A. N. Bykanov, G. O. Vaschenko, O. V. Khodykin, J. R. Hoffman, E. Vargas L., R. D. Simmons, J. A. Chavez, and C. P. Chrobak, "LPP EUV source development for HVM," in *Emerging Lithographic Technologies XI*, M. J. Lercel, Ed., *Proc. SPIE* **6517**, 65170Q (2007).
4. D. C. Brandt, I. V. Fomenkov, A. I. Ershov, W. N. Partlo, D. W. Myers, N. R. Böwering, G. O. Vaschenko, O. V. Khodykin, A. N. Bykanov, J. R. Hoffmann, C. P. Chrobak, S. N. Srivastava, D. A. Vidusek, S. De Dea, and R. R. Huo, "Laser-produced plasma source system development," in *Lithography Asia 2008*, A. C. Chen, B. Lin, A. Yen, Eds., *Proc. SPIE* **7140**, 71401E (2008).
5. I. V. Fomenkov, D. C. Brandt, A. N. Bykanov, A. I. Ershov, W. N. Partlo, D. W. Myers, N. R. Böwering, G. O. Vaschenko, O. V. Khodykin, J. R. Hoffman, E. Vargas L., R. D. Simmons, J. A. Chavez, and C. P. Chrobak, "Laser-produced plasma source system development," in *Emerging Lithographic Technologies XI*, M. J. Lercel, Ed., *Proc. SPIE* **6517**, 65173J (2007).
6. N. R. Böwering, J. R. Hoffman, O. V. Khodykin, C. L. Rettig, B. A. M. Hansson, A. I. Ershov, and I. V. Fomenkov, "Metrology of laser-produced plasma light source for EUV lithography," in *Metrology, Inspection, and Process Control for Microlithography XIX*, R. M. Silver, Ed., *Proc. SPIE* **5752**, 1248–1256 (2005).
7. N. R. Böwering, A. I. Ershov, W. F. Marx, O. V. Khodykin, B. A. M. Hansson, W. N. Partlo, E. Vargas L., J. A. Chavez, I. V. Fomenkov, D. W. Myers, and D. C. Brandt, "EUV source collector," in *Emerging Lithographic Technologies X*, M. J. Lercel, Ed., *Proc. SPIE* **6151**, 61513R (2006).
8. T. Feigl, S. Yulin, N. Benoit, M. Perske, M. Schürmann, N. Kaiser, N. R. Böwering, O. V. Khodykin, I. V. Fomenkov, and D. C. Brandt, "Enhanced reflectivity and stability of high-temperature LPP collector mirrors," in *Advances in X-Ray/EUV Optics and Components III*, A. M. Khounsary, C. Morawe, S. Goto, Eds., *Proc. SPIE* **7077**, 70771W (2008).



Norbert R. Böwering received his diploma in physics from the University of Würzburg, Germany, in 1981 and a PhD in physics from the University of Texas at Austin in 1985. He worked as a research associate and lecturer at the University of Bielefeld, Germany, where he completed the habilitation in experimental physics in 1991. Following an appointment at the Max-Born Institute, Berlin, he has worked in industry on EUV light source development since 2000 and joined Cymer in 2001. He has more than 20 years of experience in research using EUV radiation.



Igor V. Fomenkov graduated with a Master's degree and received his PhD in physics and mathematics from the Moscow Institute of Physics and Technology in 1981 and 1986, respectively. He then worked as a senior scientist at the Institute of General Physics. His research was conducted in areas of interaction of laser radiation with matter and plasma diagnostics. Since 1992, he has been with Cymer, Inc., currently as a senior member of technical staff, working on research and development of excimer lasers and novel light sources for microlithography applications.

